ACS OMEGA

Open Access

http://pubs.acs.org/journal/acsodf

Article

Carbon Nanosheets Infused with Gold Nanoparticles as an Ultrasensitive Nose for Electrochemical Arsenic Sensing

Omnarayan Agrawal, Kirti Saxena, Utkarsh Jain, Nidhi Chauhan, Hitesh Kumar Sharma, Mohammad Balal, Sudipta Roy Barman, Susmita Das, and Monalisa Mukherjee*

Cite This: *ACS Omega* 2023, 8, 48360−48369

Read Online

ACCESS | Metrics & More | Article Recommendations | Supporting Information

ABSTRACT: Herein, we introduce an eco-friendly electrochemical sensor based on melamine-enriched nitrogen-doped carbon nanosheets decorated with gold nanoparticles (Au-CNSm) for arsenic sensing. An extremely facile, low-toxicity, biocompatible, and affordable hydrothermal technique was adopted for the synthesis of the Au-CNSm nanocomposite. The Au-CNSm-integrated sensing platform was optimized for electrode composition by cyclic voltammetry (CV). Owing to the synergistic effects of melamine-enriched carbon nanosheets (CNSm) and gold nanoparticles (AuNPs), the anodic peak current increased in the Au-CNSm-modified sensing electrode as compared to the CNSm-decorated platform. A wide linear range of 0.0001−100 μM and a low detection limit of 0.0001 μM were obtained. The visual signals can be measured at a very minute concentration of 0.0001 μM (0.1 ppb) on a screen-printed carbon electrode (SPCE) modified with Au-CNSm. Hence, this electrode system clearly outperformed the previously reported studies in terms of linear range, limit of detection (LOD), and electrocatalytic activity for arsenic sensing. Interestingly, the fabricated biosensor can be developed as a point-of-care device for real-time environmental monitoring for public safety. Henceforth, owing to exceptional attributes such as portability, selectivity, and sensitivity, this device offers great promise in modeling a revolutionary new class of electrochemical sensing platforms for an ultrasensitive and reliable detection strategy for arsenite (As(III)).

1. INTRODUCTION

Arsenic contamination in drinking water is a critical global issue affecting millions of individuals and can have harmful health consequences, even at low concentrations.[1] Arsenic-contaminated groundwater is jeopardizing the health of more than 100 million people worldwide.[2] According to the World Health Organization and the United States Environmental Protection Agency, the concentration of arsenic in drinking water must be below 10 ppb.[3,4] When arsenic-containing wastewater is discharged directly into rivers through pipes, perforations, and sinkholes, it culminates in serious ailments such as lung cancer, skin cancer, myalgia, neuropathy, and genetic anomalies.[5] By comparing the natural forms of arsenic, we find that As(III) is approximately 60 times more toxic than As(V) and other organic arsenic groups.[6] Therefore, developing a delicate, quick, and accurate technique for detecting arsenic in water is subsequently essential. Extensive research work has been performed for the detection of arsenic; currently, several analytical methods are used for detecting arsenic, such as atomic fluorescence spectrometry (AFS), atomic absorption spectroscopy (AAS), capillary electrophoresis, flame AAS, high-performance liquid chromatography (HPLC), graphite furnace AAS,[7] and inductively coupled plasma mass spectrometry (ICP-MS).[8] Their application in heavy metal detection is impeded by their expensive, time-consuming, and cumbersome operating techniques, as well as the difficulty in achieving real-time detection.[9] As of present, high-grade metals like gold and platinum have been discovered to be among the most effective sensing materials to detect

Received: October 7, 2023
Revised: November 16, 2023
Accepted: November 22, 2023
Published: December 9, 2023

arsenic. For example, Zhuang[10] and team performed in situ synthesis of ZnO onto a nanoporous gold microelectrode for the electrochemical sensing of As(III) in near-neutral conditions. They have achieved a sensitivity of 1.366 μA ppb^{-1} cm^{-2} with a low limit of detection of 0.30 ppb (S/N = 3) in a concentration range of 1.0−260 ppb, while Ping's team[11] developed an Fe-MOF/MXene-based ultrasensitive electrochemical sensor for As(III) measurement by square wave anodic stripping voltammetry, with a sensitivity of 8.94 $\mu A(ng\ L^{-1})^{-1}\ cm^{-2}$ and a limit of detection as 0.58 ng L^{-1}. Furthermore, Gunasekaran et al.[12] developed electrochemical sensing of arsenic ions using a covalently functionalized benzotriazole-reduced graphene oxide-modified screen-printed carbon electrode (SPCE). Moreover, their inaptness to constantly monitor a plethora of samples entails the need for an effective sensing system to subjugate the burgeoning enigma. Carbon nanomaterials, including carbon nanodots (CNDs), fullerene, and graphene quantum dots (GQDs)-based electrodes, aid in the detection of heavy metals; however, their electrochemical applications in metal sensing are limited because of their larger surface area, high aspect ratio, and remarkable properties such as thermal and electrical conductivity. In this study, we have come up with an innovative strategy for producing heavy-metal-free electrode materials with exceptional efficacy in As(III) sensing. Melamine serves as the primary nitrogen source and is doped in the base material. During the electrochemical modification process, it becomes evident that CNSm exhibits a highly conductive nature, primarily attributed to the active sites generated by the nitrogen functional groups present on the CNSm. This research underscores the profound influence of carbonization temperature on the nitrogen content, revealing that a modest proportion of nitrogen can exert a positive influence on the conductive performance of the resulting materials, thus enhancing their capabilities in As(III) sensing. It has been demonstrated that a combination of a large specific surface area and a mesoporous structure plays a constructive role in its conductive nature.[13] This is attributed to the excellent accessibility of catalytically active sites to the electrolyte and efficient charge transport facilitated by the carbon matrix, both of which are advantageous for analyte detection. We postulate that more effective N-doping can be achieved by more suitable N-precursors. In our present investigation, we have delved into the impact of CNSm and carbonization temperature on the nitrogen content. Furthermore, we have observed that while overall high nitrogen content is significant, it is not the sole governing factor for improving the catalytic and conductive nature. The type and concentration of pyridine nitrogen and pyrrolic nitrogen are equally pivotal, and both are present in our nanocomposite, as shown by X-ray photoelectron spectroscopy (XPS) spectra in Figure 4c. Hence, carbon materials doped with nonmetal heteroatoms, specifically nitrogen integrated into the fundamental carbon structure, are of great interest. Here, we demonstrate melamine-enriched nitrogen-doped carbon nanosheets augmented with gold nanoparticles obtained hydrothermally via a simple one-pot hydrothermal method, utilizing CNSm and auric chloride solution. Notably, CNSm served as a convenient single source of the precursor, making the synthesis process easily scalable and environmentally friendly. Remarkably, this approach obviated the requirement of catalysts or organic solvents. CNSm has been revealed to be one of the most promising nanomaterials for the detection of arsenic from groundwater due to its higher adsorption capacity, sensing nature, and specificity.[14,15] Moreover, gold or gold film electrodes are considered superior in sensitivity towards arsenic oxidation to silver, platinum, or other electrode materials.[16] Au-CNSm has been employed in electrochemical sensing by coating it on the surface of electrodes to create an electrochemical interaction for the adsorption of analytes that are more sensitive, such as heavy metal ions.[17] Here, we developed Au-CNSm/SPCE having a high limit of detection (LOD) and a broad linear range toward arsenic in drinking water. Its sensing effects depend on the ability of arsenic to adsorb on the surface of the Au-CNSm hybrid, which can improve the detection limit of arsenic As(III). Electrochemical methodologies hold significant promise for the detection of heavy metal ions (HMIs) such as arsenic in environmental samples. Electrochemical approaches offer swiftness, accuracy, and accessibility. Upon exposure to variations in the electric potential, heavy metal ions with redox activity undergo oxidation on the surface of the working electrode (WE) in electrochemical systems. This oxidative process results in a rapid surge of electric current directly correlated to the concentration of HMI present in the solution. Notably, these oxidation peaks manifest at distinct oxidation potentials, facilitating the simultaneous detection and measurement of multiple HMI signals through a single voltammetric scan. Among these sensing methods, cyclic voltammetry, an electrochemical technique, is used for sensing arsenic. CV enables the electrode potential to be swept over a wide range, which is significant because arsenic species can undergo a wide range of redox reactions that cover the complete potential range in a single scan. It is also excellent for investigating arsenic's complicated electrochemical behaviors and has also gained attention due to its low cost, remarkable portability, high sensitivity, quick analysis time, and adaptability for the on-site, real-time study.[18] The Au-CNSm-modified electrode surface provides a more sensitive voltammetry response in contrast to other metallic electrode systems employed for arsenic detection.[19] The reason is that As and Au form an intermetallic complex that can boost the effectiveness of As(0).[20] Moreover, AuNPs supported on a carbon substrate reduce interference from external moieties such as the Cu(II) ion, allowing for the detection of minute concentrations of As(III).[21] Based on all of these findings, we infer that adding Au nanoparticles to the surface of carbon materials, including carbon nanosheets, may provide a possible nanomaterial for As(III) detection that is highly sensitive.[20]

2. EXPERIMENTAL SECTION

2.1. Chemical Reagent. Tetrachloroauric acid or auric chloride ($HAuCl_4$) was purchased from Sigma-Aldrich, India, and arsenic trioxide (AS_2O_3, 99%) was purchased from QualiChem's Fine Chemical Pvt., Ltd. (Gujarat, India). CNSm was prepared using the hydrothermal method of preparation. All chemicals used were of high-quality analytical grade and used as received. AS_2O_3 As(III) stock solution was prepared, and before the experiment, the As(III) solution was diluted to an appropriate concentration.

2.2. Instrumentation. Scanning electron microscopy (SEM; JEOL JSM 7500F) was employed to investigate the samples at an accelerating voltage of 5 kV. Atomic force microscopy (AFM) analysis was performed at IUAC, New Delhi, via a Nasoscope IIIa model instrument maintained under tapping mode. With the aid of a D8 Advance-Powder X-

https://doi.org/10.1021/acsomega.3c07805
ACS Omega 2023, 8, 48360−48369

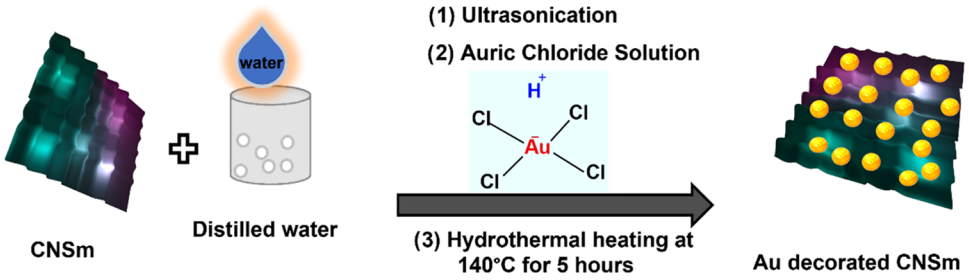

Figure 1. Schematic illustration of the synthesis of Au-CNSm from the hydrothermal reduction method.

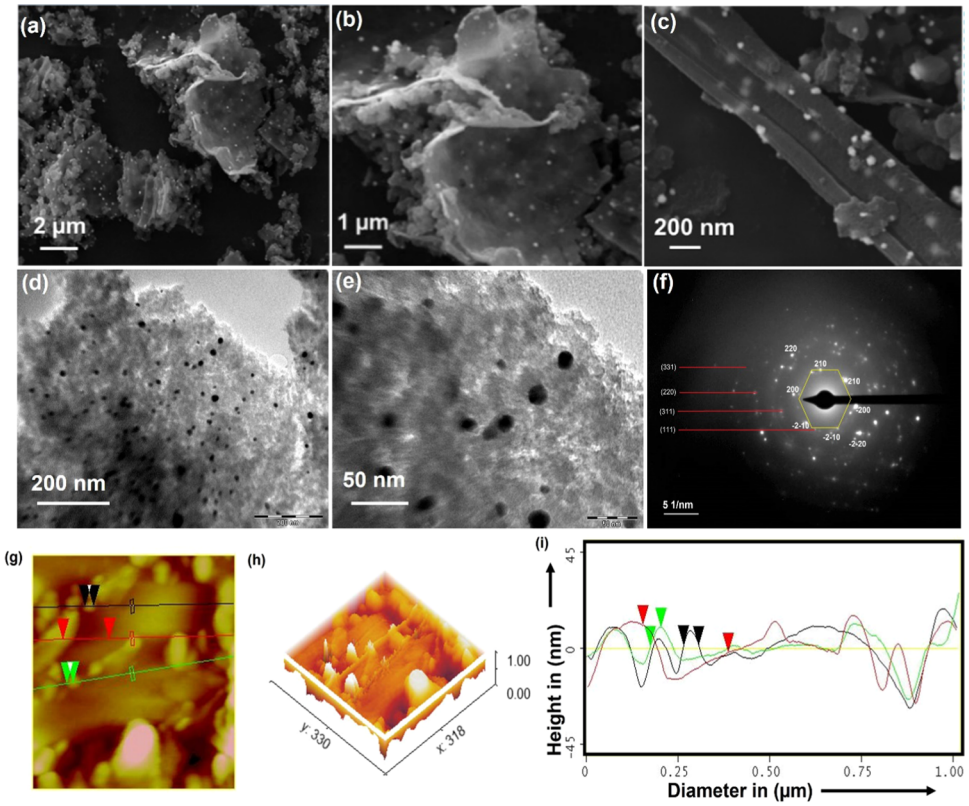

Figure 2. SEM of Au-CNSm at (a) 2 μm, (b) 1 μm, and (c) 200 nm. TEM images of Au-CNSm at (d) 200 nm and (e) 50 nm. (f) SAED pattern. AFM images of Au-CNSm deposited on freshly prepared silicon wafers: (g) 2D topographic view of Au-CNSm, (h) 3D view of Au-CNSm, and (i) corresponding height profile analysis of Au-CNSm.

ray diffractometer (XRD) and Cu Kα radiation (k = 0.154 nm) in the θ−2θ range, the structural characteristics of the Au films were determined. For surface analysis, XPS measurement was carried out at the Indus-2 beamline at RRCAT Indore with a double crystal monochromator (DCM) using a pair of Si(111) crystals. Using a HORIBA-DUETTA spectrophotometer, absorption spectra in the ultraviolet−visible (UV−vis) region were obtained in the range of 250−800 nm. Fourier transform infrared spectroscopy (FTIR) conducted by using an FTIR (UPD) spectrometer was performed in the 500−4000 cm^{-1} range. Raman spectra were collected at a 473 nm laser source on a Raman spectrometer, where the sample was laid on a metal chip. The beam of the excitation laser was directed at its surface and tailored to receive an appropriate signal from the analysis. SPCE, which was designed for the development of sensors with superior electronic transfer properties, was utilized in electrochemical studies. The working electrode (4.0 mm) is composed of carbon, along with the counter electrode, whereas the reference electrode is made up of silver. All studies were performed in air at ambient temperature (25 ± 2 °C).

2.3. Synthesis of CNSm. The synthesis of carbon nanosheets was carried out through a hydrothermal process using melamine (Merck, 98%) and glycerol (Fisher Scientific, 99%) as starting materials, and the synthesis involved a hydrothermal procedure utilizing melamine (purity: 98% from Merck) and glycerol (purity: 99% from Fisher Scientific) as precursor materials. Specifically, 0.5 g of melamine was dissolved in 10 mL of glycerol with continuous stirring at room temperature for 30 min. The resulting mixture was carefully combined with 10 mL of concentrated sulfuric acid (purity: 98% from Merck) to form a homogeneous solution. Subsequently, this solution was transferred into a 50 mL Teflon-lined stainless steel autoclave (Xiniu Tech, China) and subjected to hydrothermal treatment at 180 °C for 4 h inside a hot-air oven. This process facilitated both the carbonization of melamine and incorporation of essential nitrogen (N) configurations into the carbon framework, resulting in the

https://doi.org/10.1021/acsomega.3c07805
ACS Omega 2023, 8, 48360−48369

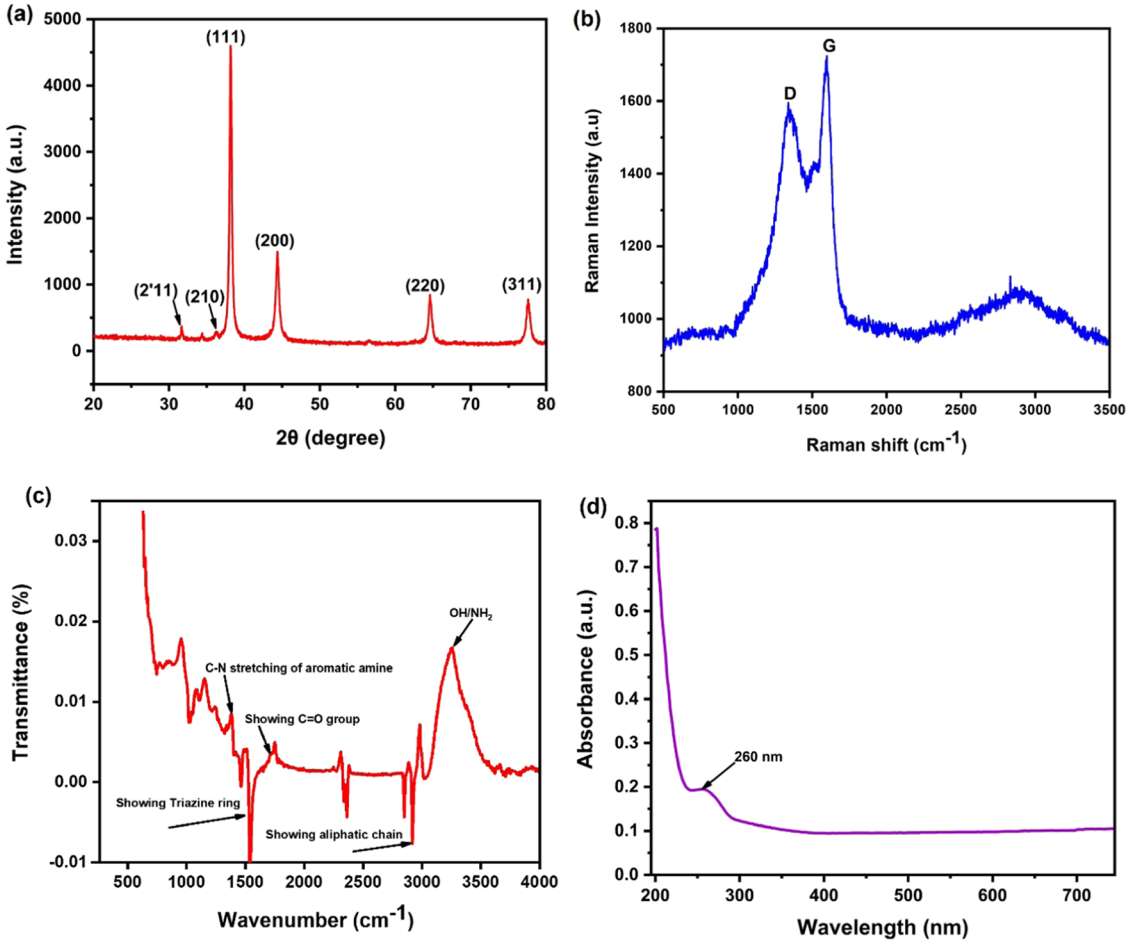

Figure 3. Characterization of Au-CNSm by (a) XRD, (b) Raman, (c) FTIR, and (d) UV−visible absorption spectra.

formation of a melamine-enriched carbon nanosheet (CNSm). The resulting product was thoroughly washed three times using a solution of acetone and distilled water (in a ratio of 10:90, v/v). Afterward, the collected material was dried at 50 °C to obtain the desired products. Prior to utilization, the as-synthesized nanomaterials were dispersed in deionized water for sterility purposes and then subjected to sonication at room temperature for 45 min to disperse any aggregates.

2.4. Preparation of the Au-CNSm Nanocomposite. The Au-CNSm nanocomposite was crafted with a hydrothermal method (in Figure 1). In a typical procedure, 15 mg of freshly prepared CNSm was mixed with 10 mL of deionized water and subjected to ultrasonication for 1 h to assist the ionic interaction. In 5 mL of water, 6 mg of $HAuCl_4{\cdot}3H_2O$ having a concentration of 1 mM was added to the aforementioned solution and further sonicated for 30 min to obtain an appropriate dispersion of CNSm with auric chloride solution.[22] We observed that the color of the mixture shifted from yellow to dark yellow, indicating the introduction of the Au-CNSm formation. This suspension was kept at room temperature for about 40 min and stirred to assist the gold ions' interaction with the CNSm surface. The solution was then transferred in a 50 mL PTFE-lined stainless steel autoclave and heated at 140 °C for 5 h to create the Au-CNSm nanocomposite. The reaction mass was centrifuged and cooled with distilled water before being used.

2.5. Electrode Modification Using an Engineered Au-CNSm Nanocomposite. Cyclic voltammograms were recorded in a three-electrode cell system at 50 mV s^{-1} using SPCE in which the carbon electrode acts as the working electrode, Ag/AgCl as the reference electrode, and a platinum wire as the counter electrode in a 5 mM $K_3Fe(CN)_6$/5 mM $K_4Fe(CN)_6$ solution as a redox probe. The SPCE system was rinsed with water and then modified by coating it with Au-CNSm. After that, 50 μL of the Au-CNSm nanocomposite suspension was drop-cast on SPCE and left overnight. The electrochemical investigation was then carried out on the modified electrode to determine various parameters. The analytical performance of the modified electrode was assessed by testing its response to different concentrations of arsenic solution, ranging from 0.0001 to 100 μM.

3. RESULTS AND DISCUSSION

3.1. Characterization of the Au-CNSm Nanocomposite. *3.1.1. Morphological Analysis.* The morphology of as-synthesized Au-CNSm was examined by scanning electron microscopy (SEM) and transmission electron microscopy (TEM). As given in Figure 2a, the SEM images describe the bright Au nanoparticles with a mean size of around 70−80 nm, which are uniformly distributed on CNSm, corroborating the successful fabrication of the AuNPs on CNSm. Figure 2b clearly shows the thin and wrinkled nanosheet of the CNSm material in which AuNPs are distributed in a heterogeneous manner, while in Figure 2c, a thin layered morphology of CNSm can be observed. The dispersion of AuNPs over CNSm within the nanocomposite was investigated by TEM. In Figure

https://doi.org/10.1021/acsomega.3c07805
ACS Omega 2023, 8, 48360−48369

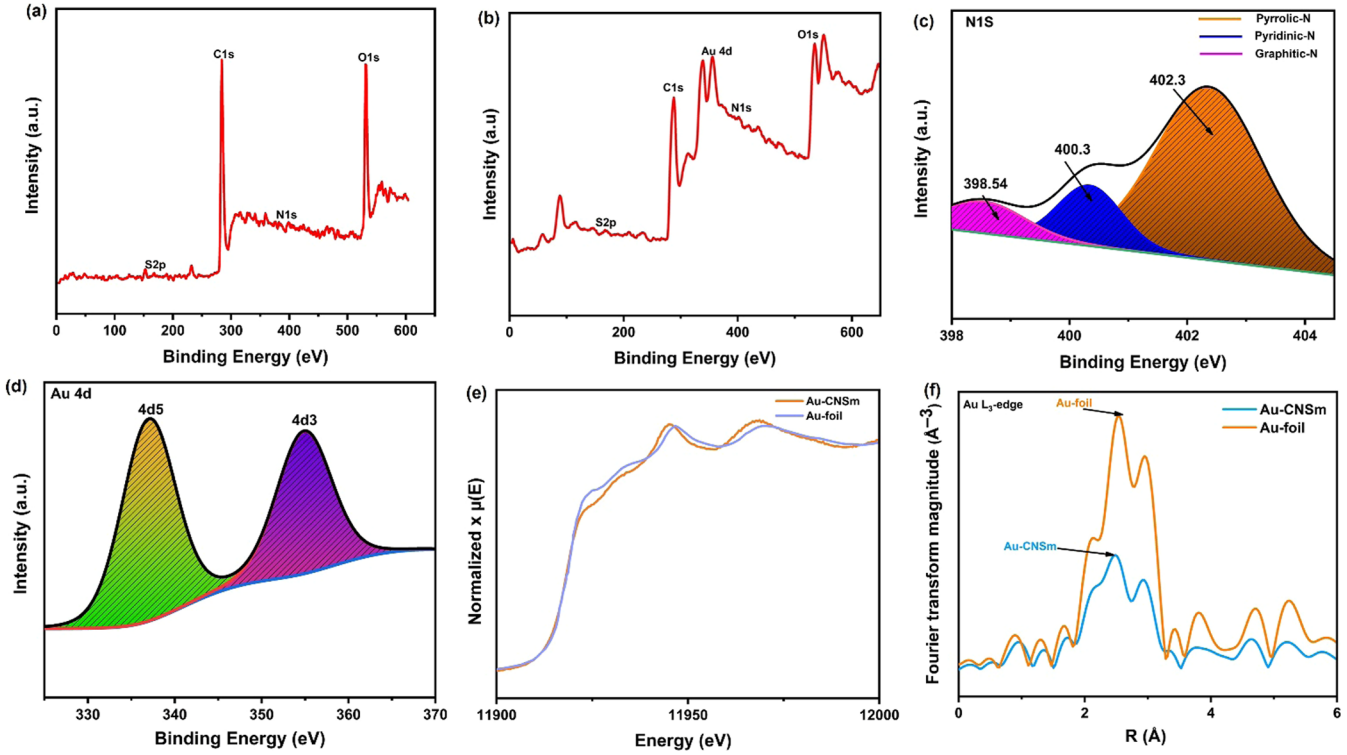

Figure 4. Survey XPS spectra of CNSm (a) and (b) Au-CNSm. High-resolution deconvoluted spectra of N 1s CNSm (c) and Au 4d spectrum of Au-CNSm (d). Normalized Au L_3-edge XANES spectra of the Au-CNSm sample with the Au foil [Au(0)] as a reference (e) and (f) Fourier transformed Au L_3-edge EXAFS spectra $\chi(R)$ versus R for Au-CNSm and Au foil.

2d, the TEM image shows the sheet-like structures of CNSm on which AuNPs are distributed. In Figure 2e, the TEM image reveals that AuNPs are well dispersed within the nanocomposite. Figure 2f exhibits a high-magnification TEM image of the Au-CNSm nanocomposite, showing a completely polycrystalline and ordered structure confirmed from the selected area electron diffraction pattern (SAED) image. Figure 2f depicts the SAED distribution of Au-CNSm. The steady patterned circle of polycrystalline carbon inside the SAED image (Figure 2f) explicitly demonstrates the creation of prevalent hexagonal symmetry, which is symbolic for turbostratic layers, specifying that CNSm has indeed been transformed into graphite and AuNPs have been stacked into the graphite layer, affirming the nucleus of Au-CNSm. The SAED pattern validates the polycrystalline nature of the Au-CNSm nanocomposite by displaying four concentrating rings, and *d*-spacings of 0.23 and 0.12 nm are consistent with the (111) and (311) lattice of the face-centered cubic form of AuNPs, respectively. The predicted crystal planes and *d*-spacing values are compared with XRD data and found to be in good agreement. The atomic force microscopy (AFM) of the nanocomposite (Figure 2g) demonstrates the two-dimensional (2D) view of Au-CNSm. Figure 2h represents the three-dimensional (3D) view of the Au-CNSm nanocomposite, and Figure 2i shows the corresponding height profile graph of the Au-CNSm nanocomposite in which the red cap represents the height of the CNSm sheet to be 12.706 nm, the green cap indicates the height of AuNPs as 8.472 nm, and the black cap denotes the diameter of AuNPs of approximately 41.314 nm. Furthermore, energy-dispersive X-ray (EDX) analysis confirms the formation of AuNPs on the CNSm surface. Figure S1(a) displays the EDX spectra of the Au-CNSm composite in which the C, O, S, and Au element peaks are visible, serving as proof of the chemical compositions of Au-CNSm. According to the integral area of each characteristic peak, the weight ratios of C, O, S, and Au are estimated to be 58.40, 23.40, 2.13, and 16.07%, respectively. The atomic ratios of C, O, S, and Au are approximately 75.12, 22.60, 1.03, and 1.26%, respectively, confirming that AuNPs were successfully electrodeposited on the Au-CNSm-modified SPCE surface.

3.1.2. Chemical Characterization of the Au-CNSm Nanocomposite. XRD analysis deduces the mechanistic elucidation of the Au-CNSm configuration from the precursor CNSm via the hydrothermal route based on modifications in the crystalline and amorphous phases. Similarly, the Au-CNSm XRD estimation of the specimen substantiates our theory concerning the influence of temperature on the crystallinity degree of the material. CNSm exhibited some amorphous nature, with a cyclohexane monoclinic carbon phase at 31.6° having (2′11) planes (JCPDS file 48-1960) and a cubic phase at 36.16° having (210) planes (JCPDS file 18−0311).[23] In the case of Au-CNSm, the cyclohexane monoclinic carbon phase declined significantly after the hydrothermal process in conjugation with AuNPs, with a concomitant increase and textured growth of the gold phase. The XRD pattern for Au-CNSm, however, is in good agreement with the reference pattern for cubic Au (JCPD 89−3697), which demonstrates all of the major peaks of Au at 38.3° (111), 44.5° (200), 64.7° (220), and 77.6° (311), confirming the decoration of AuNPs on the CNSm surface. The sharp peaks and low fwhm in Figure 3a indicate that the synthesized nanocomposite (Au-CNSm) has high crystallinity. The XRD patterns of Au-CNSm showed a gradual decrease in peak heights with a concurrent increase in peak width, which corroborated the gradual decrease in particle size.[24] Moreover, during XRD analysis of Au-CNSm, peaks exhibiting the impurities of the material were

https://doi.org/10.1021/acsomega.3c07805
ACS Omega 2023, 8, 48360−48369

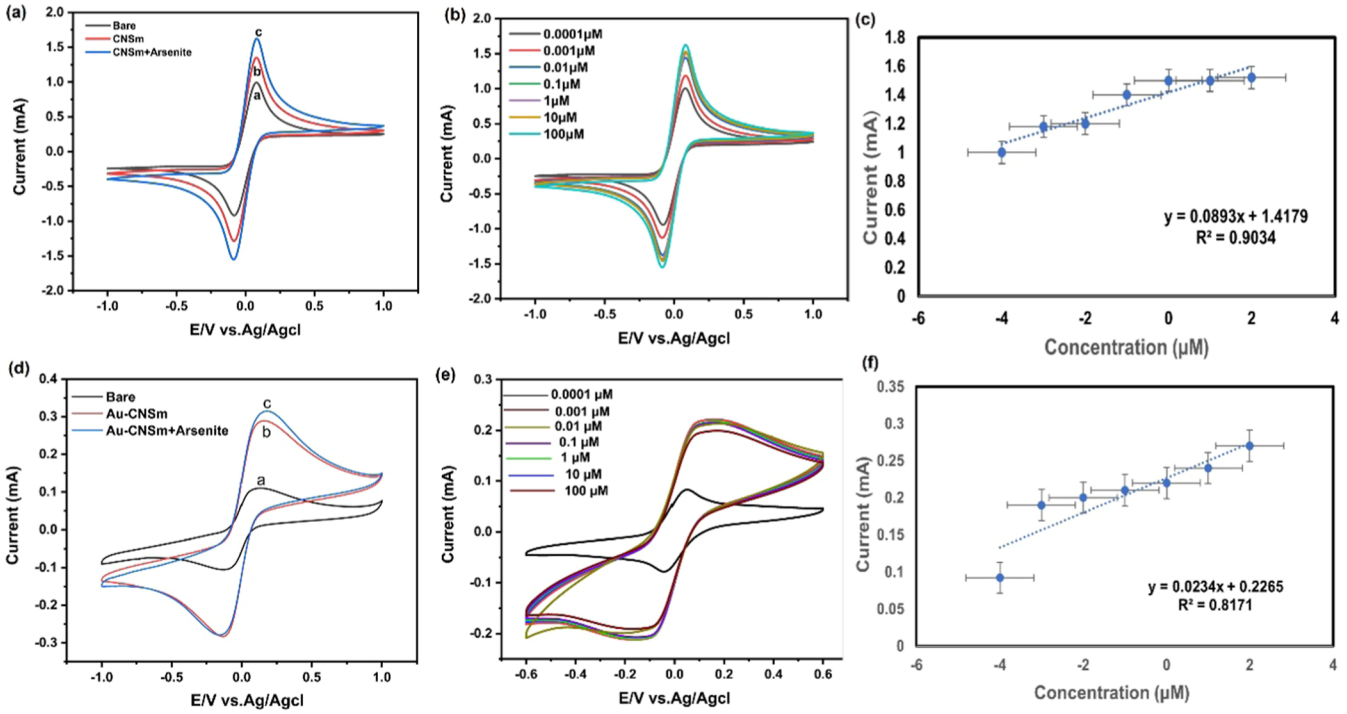

Figure 5. Cyclic voltammograms of (a) CNSm/SPCE in a 5 mM potassium ferricyanide ($K_3Fe(CN)_6$)/5 mM potassium ferrocyanide ($K_4Fe(CN)_6$) solution with 100 μM As(III) at a scan rate of 50 mV s^{-1} and (b) CNSm/SPCE at various concentrations of As(III) from 0.0001 μM to 100 μM with the 5 mM $K_3Fe(CN)_6$/5 mM $K_4Fe(CN)_6$ solution at a scan rate of 50 mV s^{-1}. (c) CNSm/SPCE shows the corresponding variation of current density as a function of concentration of As(III). Cyclic voltammograms of (d) Au-CNSm/SPCE in the 5 mM $K_3Fe(CN)_6$/5 mM $K_4Fe(CN)_6$ solution with 100 μM As(III) at a scan rate of 50 mV s^{-1} and (e) Au-CNSm/SPCE at various concentrations of As(III) from 0.0001 to 100 μM with a ferri/ferro solution at a scan rate of 50 mV s^{-1}. (f) Au-CNSm/SPCE displays the relevant current density change as a function of the concentration of As(III).

not present, supporting pristine composite formation among selected moieties. The quantitative and qualitative evaluation of structural defects, such as functional groups, doping, grain boundaries, and voids, was performed using Raman spectroscopy.[25,26] Structural changes that occurred due to the functionalization of CNSm over AuNPs can be observed by changes in Raman spectroscopy bands.[27] According to Wang et al.,[28] the Raman spectra of CNSm show two bands: the G band at 1588 cm^{-1}, which occurs from the first order scattering of the E_{2g} phonon of sp^2 carbon atoms demonstrating graphitic carbon, and other is the D band at 1370 cm^{-1}, which indicates the presence of disorder as well as the edges due to breathing mode of k-point photons with A_{1g} symmetry. In the Raman spectra of the Au-CNSm nanocomposite, the D band, which is localized at about 1339 cm^{-1}, is correlated to the vibrations of sp^3-bonded carbon atoms with defects and disorder, while the G band, which arises at around 1595 cm^{-1}, corresponds to the vibrations of sp^2-bonded carbon atoms in a hexagonal lattice. As can be seen from Figure 3b, their intensity ratio (I_D/I_G) is often used as a measure of the degree of carbon disruption. The D and G modes were characterized by the Au-CNSm's Raman spectra along with two distinct peaks at 1339 and 1595 cm^{-1}, respectively, and the strength of the G band is higher than that of the D band. The combined investigations conclude that the intensity ratio of (I_D/I_G) increased from 0.91 to 0.93, indicating a considerable reduction in the extent of the in-plane sp^2 domain and an increase in disorder. The FTIR spectra of Au-CNSm shown in Figure 3c depict how the number of functional groups associated with each other provide stability by capping them. In the FTIR spectra, the absorption peak at 1700 cm^{-1} due to the carbonyl C═O group confirms the presence of the −COOH group, while the signal at 3000−3400 cm^{-1} is related to −OH groups.[28] Triazine fingerprints between 1400 and 1600 cm^{-1} were found in CNSm samples, revealing that CNSm comprises triazine rings that were originally found in melamine and also an aliphatic chain at around 2900 cm^{-1} due to glycerol, as shown in spectra. When we analyze the FTIR spectra of Au-CNSm with AuNPs embellished on the CNSm, an extra peak at 1388 cm^{-1} is attributed to the C−N stretching vibration of aromatic amines and the C−OH stretching of the secondary alcohol, which was also observed. Figure 3d shows the UV−visible absorption spectra of Au-CNSm; AuNPs exhibit a dominant absorption band at 260 nm corresponding to $\pi-\pi^*$ transitions of carbon−carbon bonds and $n-\pi^*$ transitions of carboxyl bonds.

XPS analysis infers the interaction between CNSm and Au-CNSm along with their chemical composition. The XPS survey spectra over a broad range of binding energies (0−1200 eV) for both CNSm (in Figure 4a) and Au-CNSm (in Figure 4b) indicate a small C 1s peak at 284.5 eV, an O 1s peak at 532.5 eV, a N 1s peak at 400 eV, a S 2p peak at 167.5 eV, and a Au 4d peak at 355 eV. Figure 4b illustrates the broad-scan XPS spectrum of Au-CNSm, which reveals that the fabricated hybrid material comprises blended Au, C, O, N, and S elements. Figure 4c displays the deconvoluted spectrum of N 1s, which features two distinct convoluted peaks at 398.5 and 399.8 eV; the peak at 398.5 eV is represented by pyrrolic-N, while the other is resulted by pyridinic-N.[29] Figure 4d illustrates sharp peaks at 335.9 and 354.5 eV in the Au 4d

https://doi.org/10.1021/acsomega.3c07805
ACS Omega 2023, 8, 48360−48369

deconvoluted spectrum.[30] Correspondingly, Au 4d spectra were indexed for the two main peaks 4d3 (354.5 eV) and 4d5 (335.9 eV), which is significant to metallic gold owing to the dominance of AuNPs over CNSm, which is in corroboration with the FTIR results, emphasizing the 2D structure of the carbon nanosheets of sp^2 carbon and triazine structures. S and O atoms appeared from H_2SO_4 and adsorbed SO_2 gas, which were the byproduct of the reaction. Figure 4e shows the extended X-ray absorption fine structure (EXAFS) and X-ray absorption near edge spectroscopy (XANES) data, confirming the structure and properties of AuNPs in these materials.[31] Au L_3-edge XANES and scanning extended edge X-ray absorption fine structure (XAFS) spectra were obtained at the BL-9 (EXAFS) Indus-2 beamline. The XAFS spectra of Au samples were taken in transmission mode. The beamline is completely fabricated of a collimated Rh/Pt-wrapped meridional cylindrical mirror and a Si (111)-premised double crystal monochromator to select the excitation energy. The XANES clearly reveals both oxidized and reduced Au species. Figure 4 depicts four distinct edge characteristics. The fragile peak near 11,940 eV, which is the characteristic peak of AuNPs originally seen in the XANES, but the two peaks between 11,940 and 11,980 eV seem to be more structure-dependent. The peaks between 11,925 and 11,980 eV imply that XANES is affected by parameters such as the concentration of AuNPs and the structure of the host element. The energy range of XAFS was calibrated using a Au metal foil at 11,919 eV. Figure 4e shows the normalized Au L_3 edge spectra of CNSm. From XANES measurements, one may observe that the CNSm sample has a Au(0) oxidation state. Figure 4f shows the Fourier transform (FT) of the XAFS spectra of CNSm samples in comparison with the Au metal. In the Fourier transform of the extended X-ray fine structure (EXAFS) signal, the first peak of Au-CNSm appears at 2.48 Å, which is slightly lower than the interatomic distance (R) value of the reference Au foil complex. It emerges due to the presence of different characteristics of gold ligands. Owing to the inherent constraints of the analytical technique and the inadequate data integrity for EXAFS quantification, it is difficult to distinguish the prevalence of tiny gold clusters or other multimetallic complexes from the X-ray absorption data. The existence of these small gold clusters could be highlighted by the modest peaks at 2.54 and 2.94 Å in Figure 4f, but all these peaks may also originate from other compounds and nanostructures in the sample. Moreover, the R-space spectra of the Au L_3-edge reveal a similar configuration as that of the gold foil, which clearly indicates that the gold atom is metallic with zero valence. Moreover, the intersite distance[32] between gold nanoparticles is less as compared to the gold foil, as confirmed by the Y-axis of Figure 4f. All of this evidence indicates that the gold nanoparticles are successfully formed in N-rich carbon.

4. ELECTROCHEMICAL CHARACTERIZATION

The electrical conductivity of a material is determined by its capacity to carry charge carriers and the ease with which these carriers can move from one layer to another. Addressing this issue, current versus potential measurements were conducted for CNSm and Au-CNSm.

4.1. Adsorption Mechanism of As(III) on Au-CNSm. Upon modification of the SPCE with the Au-CNSm nanocomposite in the presence of 100 μM As(III) within a 5 mM $K_3Fe(CN)_6$/5 mM $K_4Fe(CN)_6$ solution, a noticeable difference in the electrochemical response was observed. In Figure 5d, the unmodified SPCE exhibited a modest current response, approximately 0.10 mA. However, following the nanocomposite (Au-CNSm) modification, a significant increase in peak current (0.3 mA) was evident. This enhancement in current can be attributed to the excellent conductivity of Au-CNSm. This enhanced conductivity is primarily attributed to the formation of an intermetallic complex between arsenic (As) and gold (Au), which, in turn, amplifies the effectiveness of As(0).[20] The formation of gold nanoparticles is further substantiated by the extended X-ray absorption fine structure (EXAFS) data presented in Figure 4e,f. This collective evidence strongly supports the successful formation of gold nanoparticles within the nitrogen-rich carbon matrix.

4.2. Electrochemical Behavior of As(III) at the Base Material CNSm-Modified Electrode. The electrochemical presence of CNSm/SPCE to As(III) was investigated by using cyclic voltammetry. Figure 5a displays the cyclic voltammetry response for bare SPCE, CNSm, and CNSm with 100 μM arsenite in a 5 mM $K_3Fe(CN)_6$/5 mM $K_4Fe(CN)_6$ solution. Bare SPCE shows an oxidation peak current of ∼0.98 mA. After the deposition of CNSm, a considerable peak current of ∼1.33 mA was attained due to the high conductivity of CNSm. The peak current value for CNSm in the presence of arsenite was obtained as ∼1.62 mA, indicating that the oxidation of the working electrode increased from As(0) to As(III). In the case of reverse scanning, the reduction peak for CNSm with arsenite was observed at −1.54 mA, while it was observed at −0.91 mA with bare SPCE. This study mainly focuses on the oxidation peak rather than the reduction peak, as the oxidation peak is more vulnerable to changes. The working electrode shows an optimum current response in the presence of As(III) due to an increase in its catalytic properties toward As(III).

4.3. Effect of Different Concentrations on the CNSm/SPCE Electrode. Various concentrations of the arsenic analyte were studied in a range from 0.0001 to 100 μM to study the electrochemical behavior and properties of arsenic species in a solution. To study the concentration effect on an electrode surface, the electrochemical CV technique was carried out. By varying the concentration of arsenic species in the solution, we can examine how the rates of electron transfer and reaction kinetics are affected. Different concentrations lead to changes in reaction rates, which can provide insights into the mechanisms and pathways of redox reactions involving arsenic. All of the evaluations were performed in a 5 mM $K_3Fe(CN)_6$/5 mM $K_4Fe(CN)_6$ solution with a scan rate of 50 mV s^{-1}. Figure 5b illustrates the CV graph for varying concentrations, where the current value was enhanced in the case of a higher concentration, whereas it decreased with the decreasing concentration. The highest current value (1.62 mA) was obtained at the maximum concentration (100 μM) due to the increased catalytic activity at the modified sensing platform. A calibration curve was also generated for arsenic concentrations from 0.0001 to 100 μM in Figure 5c. The results proved that CNSm/SPCE responded linearly between the working electrode current value and the As(III) concentration. LOD determined by CV was 0.0001 μM, and the fitted linear equation obtained was $y = 0.0893x + 1.479$ with a correlation coefficient of 0.9034.

4.4. As(III) Electrochemical Performance at the Au-CNSm Nanocomposite-Modified Electrode. To evaluate the electrochemical response of Au-CNSm/SPCE toward As(III), the cyclic voltammetry study has been carried out. Figure 5d shows the cyclic voltammetry response for

https://doi.org/10.1021/acsomega.3c07805
ACS Omega 2023, 8, 48360−48369

Table 1. Comparison of the Advanced Analytics of the As(III) Electrochemical Estimation Based on Metal/Metal Oxide-Decorated Electrodes Published in the Literature

s. no.	type of sensor	technique	linear range	limit of detection	sensitivity	references
1	AuNPs/g-C_3N_4	linear sweep anodic stripping voltammetry	0.005−1.0 μM	2.9 nM		21
2	IrO_2 nanotube/GCE	differential pulse voltammetry (DPV)		0.1 μM	0.0038 μM^{-1}	33
3	graphite electrode/Au	stripping voltammetry		17 μM		34
4	AuNPs/carbon film	anodic stripping voltammetry	1−100 ppb	0.55 ppb		35
5	gold film/plastic electrode	(DPV)	5−150 ppb	5 ppb		36
6	silver electrode	ASV		0.6 μM^{-1}	2.6 μM^{-1}	37
7	Au electrode	ASC	100−1000 ppb	75 ppb		38
8	AuNP/Ppy-NW	CV		0.32 μM	0.22 and 0.48 μM^{-1}	39
9	Au-CNSm over SPCE	CV	0.0001−100 μM	0.0001 μM		our work

modification of SPCE with the Au-CNSm nanocomposite in the presence of 100 μM As(III) in the 5 mM $K_3Fe(CN)_6$/5 mM $K_4Fe(CN)_6$ solution. In the figure, the bare electrode (SPCE) showed a current response of ∼0.10 mA. After modification with the nanocomposite (Au-CNSm), a significant increase in peak current was obtained (0.28 mA) due to the high conductivity of Au-CNSm. After the addition of 100 μM As(III), a spike in the peak current value was observed (∼0.3 mA). In the case of reverse scanning, the reduction peak appeared at ∼−0.25 mA for Au-CNSm with arsenite, while with bare SPCE, it is observed at ∼−0.13 mA. The results showed that a significant increase in peak current was obtained in the case of the Au-CNSm nanocomposite as compared to the CNSm-doped material alone.

4.5. Effect of Different Concentrations on the Au-CNSm/SPCE Electrode. The effect of different As(III) concentrations on the Au-CNSm-coated SPCE was investigated in the range of 0.0001−100 μM. A cyclic voltammetry (CV) study was conducted in a 5 mM $K_3Fe(CN)_6$/5 mM $K_4Fe(CN)_6$ solution to determine the minimum detectable concentration using the modified electrode at a scan rate of 50 mV s^{-1}. As(III) solution concentrations ranging from 0.0001 to 100 μM were drop-cast on SPCE containing the Au-CNSm-modified electrode. Different concentrations are tested to determine the LOD and limit of quantification (LOQ) for arsenic detection. These parameters define the lowest concentration at which reliable measurements can be made. This process was allowed for all different concentrations of As(III), and electrodes were washed every time before proceeding with the electrochemical experiments. Figure 5e illustrates the CV graph for varying concentrations. It was evaluated that the current value is enhanced in the case of increasing concentration, whereas it decreases with decreasing concentration. A calibration curve was also generated for arsenic concentrations from 0.0001 to 100 μM in Figure 5f, showing the results that Au-CNSm/SPCE responds linearly between the working electrode current value and the As(III) concentration. A higher current value (0.22 mA) was obtained at a maximum concentration (100 μM) due to the surge in the catalytic activity of the electrode. The proposed sensor showed a linear range from 0.0001 to 100 μM and an LOD of 0.0001 μM.

Table 1 presents a comparison of the analytical performances of different metal/metal oxide-decorated modified electrodes for calculating LOD and linear range value for As(III), where it shows that our Au-CNSm/SPCE-based sensor used for As(III) has higher LOD and linear range values than other previously reported modified electrode systems.

5. CONCLUSIONS

This study presents a method for synthesizing Au-CNSm through the utilization of an aqueous solution of $HAuCl_4$ and CNSm. The hydrothermal technique played a crucial role as a reducing agent, ensuring the stabilization of metal nanoparticles (NPs). Moreover, the synthesized particles demonstrated long-term stability. To circumvent the flaws in existing heavy metal sensing methods, an electrochemical sensor with gold nanoparticle-adorned CNSm was fabricated, an electrochemical sensor modified with a Au-CNSm nanocomposite device, which is fast, inexpensive, and convenient. Furthermore, cyclic voltammetry experiments suggest that Au-CNSm/SPCE operated well for As(III) analysis with a detection limit of 0.0001 μM (0.1 PPb), which was appropriate to analyze As(III) at levels lower than the WHO-recommended level (10 PPb). The electrode exhibits a promising utilization perspective for quick real-time analysis of samples without the interference of Cu(II) ions, with a very minuscule percentage of As(III). The results obtained from Au-CNSm/SPCE were incredibly precise and stable. The Au-CNSm/SPCE-based sensor devised for As(III) sensing exhibits superiority over other metal/metal oxide-decorated carbon nanosheet-modified electrode detectors. The intriguing results can be attributed to the potential benefit of the Au-CNSm/SPCE hybrid sensing platform for detecting As(III) in water.

■ ASSOCIATED CONTENT

Data Availability Statement

The data sets used and/or analyzed during the current study are available from the corresponding author upon reasonable request.

Supporting Information

The Supporting Information is available free of charge at https://pubs.acs.org/doi/10.1021/acsomega.3c07805.

EDX analysis (Figure S1) (PDF)

■ AUTHOR INFORMATION

Corresponding Author

Monalisa Mukherjee − *Amity Institute of Click Chemistry Research and Studies, Amity University Uttar Pradesh (AUUP), Noida, Uttar Pradesh 201303, India;* orcid.org/0000-0002-7493-0409; Phone: +91-9873279964; Email: mmukherjee@amity.edu

Authors

Omnarayan Agrawal − *Amity Institute of Click Chemistry Research and Studies, Amity University Uttar Pradesh*

https://doi.org/10.1021/acsomega.3c07805
ACS Omega 2023, 8, 48360−48369

(AUUP), Noida, Uttar Pradesh 201303, India; orcid.org/0000-0001-6036-0620

Kirti Saxena − *Amity Institute of Nanotechnology, Amity University Uttar Pradesh (AUUP), Noida, Uttar Pradesh 201303, India*

Utkarsh Jain − *School of Health Sciences & Technology (SoHST), University of Petroleum and Energy Studies (UPES), Dehradun 248007, India;* orcid.org/0000-0003-3901-0153

Nidhi Chauhan − *School of Health Sciences & Technology (SoHST), University of Petroleum and Energy Studies (UPES), Dehradun 248007, India*

Hitesh Kumar Sharma − *Amity Institute of Pharmacy, Amity University Uttar Pradesh (AUUP), Noida, Uttar Pradesh 201303, India*

Mohammad Balal − *UGC-DAE Consortium for Scientific Research, Indore, Madhya Pradesh 452001, India*

Sudipta Roy Barman − *UGC-DAE Consortium for Scientific Research, Indore, Madhya Pradesh 452001, India*

Susmita Das − *Amity Institute of Applied Sciences, Amity University-Kolkata Campus, Kolkata, West Bengal 700135, India;* orcid.org/0000-0002-9239-9463

Complete contact information is available at: https://pubs.acs.org/10.1021/acsomega.3c07805

Author Contributions

O.A.: methodology, investigation, writing—original draft, and data analysis. K.S.: performed cyclic voltammetry and helped with data analysis. U.J.: software and analysis. N.C.: conceptualization and electrochemistry. H.K.S.: editing and referencing. M.B.: XPS analysis S.R.B.: helped with getting XPS facility. S.D.: analysis and AFM. M.M.: conceptualization, supervision, visualization, methodology, writing—original draft, writing—review and editing, project administration, and funding acquisition.

Notes

The authors declare no competing financial interest.

■ ACKNOWLEDGMENTS

This work was supported by UGC-DAE CSR Government of India (IC/BL-59/CRS-176/2016−17/840). The authors also thank Amity University Noida, Uttar Pradesh, India, for providing us with research facilities and laboratory space, Smt. Babita Vinayak Salaskar from Beamline Development and application section, BARC for EXAFS measurements, and Mrs Radhika Chaurasia from Amity University, Noida, for their valuable support.

■ REFERENCES

(1) Acharyya, S. K.; Chakraborty, P.; Lahiri, S.; Raymahashay, B. C.; Guha, S.; Bhowmik, A. Arsenic Poisoning in the Ganges Delta. *Nature* **1999**, *401* (6753), No. 545, DOI: 10.1038/44052.

(2) Sarkar, S.; Blaney, L. M.; Gupta, A.; Ghosh, D.; SenGupta, A. K. Arsenic Removal from Groundwater and Its Safe Containment in a Rural Environment: Validation of a Sustainable Approach. *Environ. Sci. Technol.* **2008**, *42* (12), 4268−4273.

(3) Behari, J. R.; Prakash, R. Determination of Total Arsenic Content in Water by Atomic Absorption Spectroscopy (AAS) Using Vapour Generation Assembly (VGA). *Chemosphere* **2006**, *63* (1), 17−21.

(4) Wang, J. S.; Wai, C. M. Arsenic in Drinking Water—A Global Environmental Problem. *J. Chem. Educ.* **2004**, *81* (2), No. 207, DOI: 10.1021/ed081p207.

(5) Zhang, L.; Qin, X.; Tang, J.; Liu, W.; Yang, H. Review of Arsenic Geochemical Characteristics and Its Significance on Arsenic Pollution Studies in Karst Groundwater, Southwest China. *Appl. Geochem.* **2017**, *77*, 80−88.

(6) Feng, L.; Cao, M.; Ma, X.; Zhu, Y.; Hu, C. Superparamagnetic High-Surface-Area Fe3O4 Nanoparticles as Adsorbents for Arsenic Removal. *J. Hazard. Mater.* **2012**, *217-218*, 439−446.

(7) B'hymer, C.; Caruso, J. A. Arsenic and Its Speciation Analysis Using High-Performance Liquid Chromatography and Inductively Coupled Plasma Mass Spectrometry. *J. Chromatogr. A* **2004**, *1045* (1−2), 1−13, DOI: 10.1016/j.chroma.2004.06.016.

(8) Musil, S.; Pétursdóttir, Á. H.; Raab, A.; Gunnlaugsdóttir, H.; Krupp, E.; Feldmann, J. Speciation without Chromatography Using Selective Hydride Generation: Inorganic Arsenic in Rice and Samples of Marine Origin. *Anal. Chem.* **2014**, *86* (2), 993−999.

(9) Yogarajah, N.; Tsai, S. S. H. Detection of Trace Arsenic in Drinking Water: Challenges and Opportunities for Microfluidics. *Environ. Sci.: Water Res. Technol.* **2015**, *1* (4), 426−447.

(10) Zhuang, Z.; Chen, Y.; Chen, K.; Liu, Z.; Guo, Z.; Huang, X. In-Situ Synthesis of ZnO onto Nanoporous Gold Microelectrode for the Electrochemical Sensing of Arsenic(III) in near-Neutral Conditions. *Sens. Actuators, B* **2023**, *378*, No. 133184.

(11) Xiao, P.; Zhu, G.; Shang, X.; Hu, B.; Zhang, B.; Tang, Z.; Yang, J.; Liu, J. An Fe-MOF/MXene-Based Ultra-Sensitive Electrochemical Sensor for Arsenic (III) Measurement. *J. Electroanal. Chem.* **2022**, *916*, No. 116382.

(12) Gunasekaran, B. M.; Rayappan, J. B. B.; Rajendran, G. K.; Gopalakrishnan, G.; Nesakumar, N.; Muthiah, S.; Sivanesan, J. R. Electrochemical Sensing of Arsenic Ions Using a Covalently Functionalized Benzotriazole-Reduced Graphene Oxide-Modified Screen-Printed Carbon Electrode. *ChemistrySelect* **2022**, *7* (25), No. e202201169.

(13) Skorupska, M.; Ilnicka, A.; Lukaszewicz, J. P. The Effect of Nitrogen Species on the Catalytic Properties of N-Doped Graphene. *Sci. Rep.* **2021**, *11* (1), No. 23970.

(14) Purrostam, S.; Rahimi-Ahar, Z.; Babapoor, A.; Nematollahzadeh, A.; Salahshoori, I.; Seyfaee, A. Melamine Functionalized Mesoporous Silica SBA-15 for Separation of Chromium (VI) from Wastewater. *Mater. Chem. Phys.* **2023**, *307*, No. 128240.

(15) Zhang, J.-T.; Jin, Z.-Y.; Li, W.-C.; Dong, W.; Lu, A.-H. Graphene Modified Carbon Nanosheets for Electrochemical Detection of Pb (II) in Water. *J. Mater. Chem. A* **2013**, *1* (42), 13139−13145.

(16) Dai, X.; Nekrassova, O.; Hyde, M. E.; Compton, R. G. Anodic Stripping Voltammetry of Arsenic (III) Using Gold Nanoparticle-Modified Electrodes. *Anal. Chem.* **2004**, *76* (19), 5924−5929.

(17) Wang, C.; Yu, C. Detection of Chemical Pollutants in Water Using Gold Nanoparticles as Sensors: A Review. *Rev. Anal. Chem.* **2013**, *32* (1), 1−14, DOI: 10.1515/revac-2012-0023.

(18) De Penning, R.; Padalkar, S. Heavy Metal Sensing in Water Using Electrochemically Reduced Graphene Oxide. *MRS Commun.* **2023**, *13*, 531−537, DOI: 10.1557/s43579-023-00369-8.

(19) Majid, E.; Hrapovic, S.; Liu, Y.; Male, K. B.; Luong, J. H. T. Electrochemical Determination of Arsenite Using a Gold Nanoparticle Modified Glassy Carbon Electrode and Flow Analysis. *Anal. Chem.* **2006**, *78* (3), 762−769.

(20) Li, W.-W.; Kong, F.-Y.; Wang, J.-Y.; Chen, Z.-D.; Fang, H.-L.; Wang, W. Facile One-Pot and Rapid Synthesis of Surfactant-Free Au-Reduced Graphene Oxide Nanocomposite for Trace Arsenic (III) Detection. *Electrochim. Acta* **2015**, *157*, 183−190.

(21) Bu, L.; Xie, Q.; Ming, H. Gold Nanoparticles Decorated Three-Dimensional Porous Graphitic Carbon Nitrides for Sensitive Anodic Stripping Voltammetric Analysis of Trace Arsenic (III). *J. Alloys Compd.* **2020**, *823*, No. 153723.

(22) Chang, C.-C.; Wu, H.-L.; Kuo, C.-H.; Huang, M. H. Hydrothermal Synthesis of Monodispersed Octahedral Gold Nanocrystals with Five Different Size Ranges and Their Self-Assembled Structures. *Chem. Mater.* **2008**, *20* (24), 7570−7574.

(23) Sangam, S.; Gupta, A.; Shakeel, A.; Bhattacharya, R.; Sharma, A. K.; Suhag, D.; Chakrabarti, S.; Garg, S. K.; Chattopadhyay, S.; Basu, B.; et al. Sustainable Synthesis of Single Crystalline Sulphur-Doped Graphene Quantum Dots for Bioimaging and Beyond. *Green Chem.* **2018**, *20* (18), 4245−4259.
(24) Sen, I. K.; Maity, K.; Islam, S. S. Green Synthesis of Gold Nanoparticles Using a Glucan of an Edible Mushroom and Study of Catalytic Activity. *Carbohydr. Polym.* **2013**, *91* (2), 518−528.
(25) Agarwal, A.; Jeevanandham, S.; Kar, C.; Rai, M. P.; Kumar, V.; Bohidar, H. B.; Biswas, S.; Mukherjee, M. Crystalline Domains Nested on Two-Dimensional Nanosheets as Heterogeneous Nanomachineries for the Sustainable Production of Bioactive Compounds from Chlorella Sorokiniana. *ACS Sustainable Chem. Eng.* **2022**, *10* (30), 9732−9748.
(26) Ganesan, K.; Ghosh, S.; Krishna, N. G.; Ilango, S.; Kamruddin, M.; Tyagi, A. K. A Comparative Study on Defect Estimation Using XPS and Raman Spectroscopy in Few Layer Nanographitic Structures. *Phys. Chem. Chem. Phys.* **2016**, *18* (32), 22160−22167.
(27) Satyanarayana, M.; Goud, K. Y.; Reddy, K. K.; Gobi, K. V. Biopolymer Stabilized Nanogold Particles on Carbon Nanotube Support as Sensing Platform for Electrochemical Detection of 5-Fluorouracil in-Vitro. *Electrochim. Acta* **2015**, *178*, 608−616.
(28) Wang, W.; Chakrabarti, S.; Chen, Z.; Yan, Z.; Tade, M. O.; Zou, J.; Li, Q. A Novel Bottom-up Solvothermal Synthesis of Carbon Nanosheets. *J. Mater. Chem. A* **2014**, *2* (7), 2390−2396.
(29) Li, X.; Kurasch, S.; Kaiser, U.; Antonietti, M. Synthesis of Monolayer-patched Graphene from Glucose. *Angew. Chem., Int. Ed.* **2012**, *51* (38), 9689−9692.
(30) Sun, Y.; Qi, T.; Jin, Y.; Liang, L.; Zhao, J. A Signal-on Fluorescent Aptasensor Based on Gold Nanoparticles for Kanamycin Detection. *RSC Adv.* **2021**, *11* (17), 10054−10060.
(31) Godfrey, I. J.; Dent, A. J.; Parkin, I. P.; Maenosono, S.; Sankar, G. Structure of Gold−Silver Nanoparticles. *J. Phys. Chem. C* **2017**, *121* (3), 1957−1963.
(32) Jin, Z.; Li, P.; Meng, Y.; Fang, Z.; Xiao, D.; Yu, G. Understanding the Inter-Site Distance Effect in Single-Atom Catalysts for Oxygen Electroreduction. *Nat. Catal.* **2021**, *4* (7), 615−622.
(33) Mafakheri, E.; Salimi, A.; Hallaj, R.; et al. Synthesis of Iridium Oxide Nanotubes by Electrodeposition into Polycarbonate Template: Fabrication of Chromium (III) and Arsenic (III) Electrochemical Sensor. *Electroanalysis* **2011**, *23* (10), 2429−2437, DOI: 10.1002/elan.201100332.
(34) Kamenev, A. I.; Orlov, S. E.; Lyakhov, A. B. Electrochemical Preconcentration of Arsenic (III) in Its Determination by Stripping Voltammetry at Graphite Electrodes Modified with Gold and Copper. *J. Anal. Chem.* **2001**, *56*, 850−855.
(35) Kato, D.; Kamata, T.; Kato, D.; Yanagisawa, H.; Niwa, O. Au Nanoparticle-Embedded Carbon Films for Electrochemical As3 + Detection with High Sensitivity and Stability. *Anal. Chem.* **2016**, *88* (5), 2944−2951, DOI: 10.1021/acs.analchem.6b00136.
(36) Wang, W.; Bao, N.; Yuan, W.; Si, N.; Bai, H.; Li, H.; Zhang, Q. Simultaneous Determination of Lead, Arsenic, and Mercury in Cosmetics Using a Plastic Based Disposable Electrochemical Sensor. *Microchem. J.* **2019**, *148*, 240−247.
(37) Yang, M.; Li, P.-H.; Xu, W.-H.; Wei, Y.; Li, L.-N.; Huang, Y.-Y.; Sun, Y.-F.; Chen, X.; Liu, J.-H.; Huang, X.-J. Reliable Electrochemical Sensing Arsenic(III) in Nearly Groundwater PH Based on Efficient Adsorption and Excellent Electrocatalytic Ability of AuNPs/CeO2-ZrO2 Nanocomposite. *Sens. Actuators, B* **2018**, *255*, 226−234.
(38) Marei, M. M.; Kaht, K. L.; Roussel, T. J.; Keynton, R. S.; Baldwin, R. P. Measurement of As(III) with in Situ Subtraction of Background and Interferent Signals by Double Potential Step-Anodic Stripping Coulometry. *Sens. Actuators, B* **2019**, *301*, No. 127005.
(39) Salunke, R. S.; Kasar, C. K.; Bangar, M. A.; Chavan, P. G.; Shirale, D. J. Electrodeposition of Gold Nanoparticles Decorated Single Polypyrrole Nanowire for Arsenic Detection in Potable Water: A Chemiresistive Sensor Device. *J. Mater. Sci.: Mater. Electron.* **2017**, *28*, 14672−14677.

https://doi.org/10.1021/acsomega.3c07805
ACS Omega 2023, 8, 48360−48369